iScience

CellPress
OPEN ACCESS

Article

Computational modeling of mast cell tryptase family informs selective inhibitor development

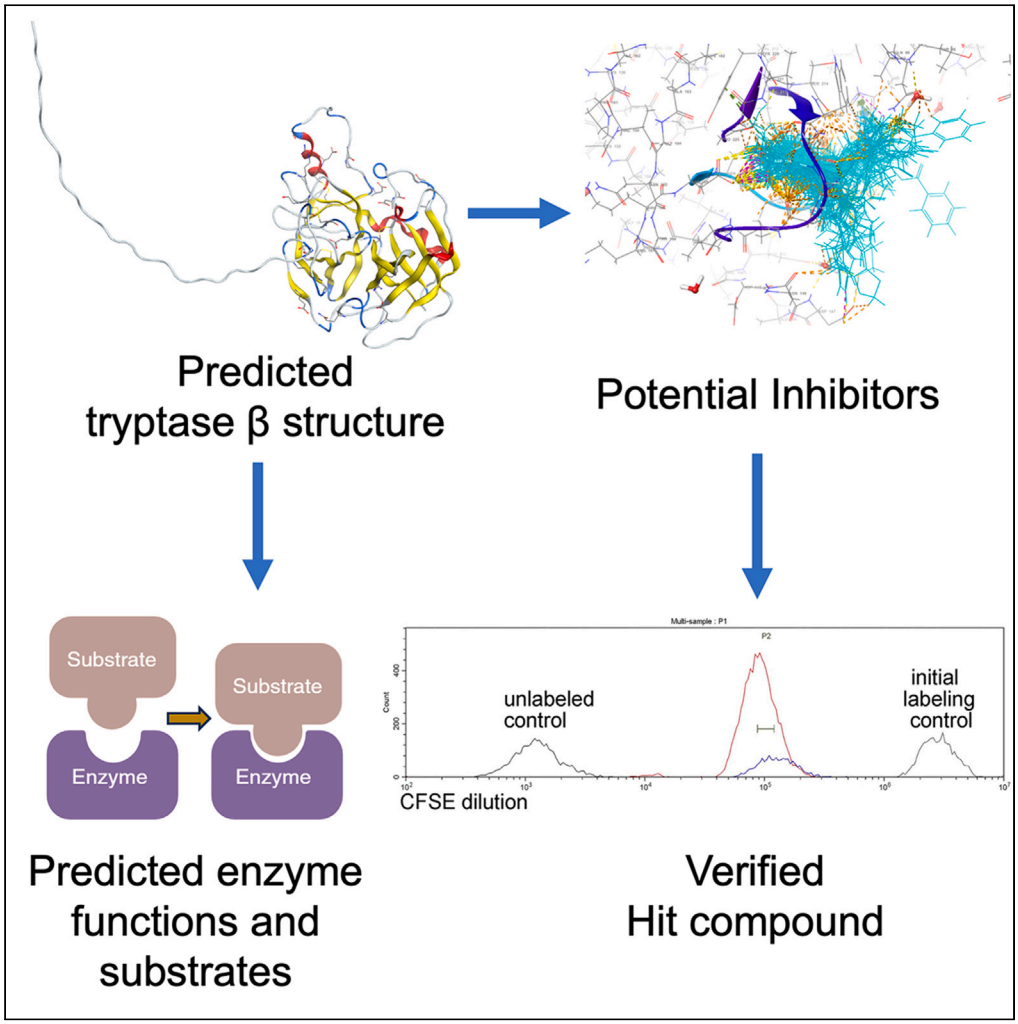

Ying Ma, Bole Li, Xiangqin Zhao, ..., Lulu Wang, Shuai Meng, Jihui Hao

yingma_maying@hotmail.com (Y.M.)
mengshuai2011@126.com (S.M.)
haojihui@tjmuch.com (J.H.)

Highlights

Computer modeling reveals structural details of all major mast cell tryptase isoforms

Unique catalytic functions identified for each tryptase isoform

High-affinity small molecule inhibitors discovered for tryptase isoforms

Experimental validation and future insights for tryptase research

Ma et al., iScience 27, 110739
September 20, 2024
https://doi.org/10.1016/j.isci.2024.110739

iScience

CellPress
OPEN ACCESS

Article

Computational modeling of mast cell tryptase family informs selective inhibitor development

Ying Ma,[1,5,6,*] Bole Li,[2,5] Xiangqin Zhao,[1,5] Yi Lu,[1] Xuesong Li,[1] Jin Zhang,[3] Yifei Wang,[1] Jie Zhang,[2] Lulu Wang,[4] Shuai Meng,[2,*] and Jihui Hao[1,*]

SUMMARY

Mast cell tryptases, a family of serine proteases involved in inflammatory responses and cancer development, present challenges in structural characterization and inhibitor development. We employed state-of-the-art protein structure prediction algorithms to model the three-dimensional structures of tryptases α, β, δ, γ, and ε with high accuracy. Computational docking identified potential substrates and inhibitors, suggesting overlapping yet distinct activities. Tryptases β, δ, and ε were predicted to act on phenolic compounds, with β and ε additionally hydrolyzing cyanides. Tryptase δ may possess unique formyl-CoA dehydrogenase activity. Virtual screening revealed 63 compounds exhibiting strong binding to tryptase β (TPSB2), 12 exceeding the affinity of the known inhibitor. Notably, the top hit (3-chloro-4-methylbenzimidamide) displayed over 10-fold selectivity for tryptase β over other isoforms. Our integrative approach combining protein modeling, functional annotation, and molecular docking provides a framework for characterizing tryptase isoforms and developing selective inhibitors of therapeutic potential in inflammatory and cancer conditions.

INTRODUCTION

IgE-dependent (such as allergens)[1,2] and IgE-independent (such as substance P or cytokines)[3] stimulation of mast cells lead to degranulation,[4] resulting in the release of tryptase-β, along with other granule enzymes and histamine. Our previous work has shown that these factors play a role in fibrosis and extracellular matrix turnover,[5] and especially, tryptase has been implicated in various diseases, including asthma and other lung disorders, inflammatory conditions, autoimmune diseases, fibrotic disorders, and cancer.[5–8] Recent reports[9,10] have linked tryptase to tumor microenvironment, involving the formation of tumor-associated fibroblasts. It also contributes to the highly fibrotic nature of cancer stroma,[5] immune cascade,[11] lack of blood supply, and hypoxia, which are significant factors contributing to poor drug efficacy and rapid chemo-resistance.

Tryptases, also known as mast cell tryptases, mast cell protease II, skin tryptase, lung tryptase, pituitary tryptase, mast cell neutral protease, and mast cell serine proteinase II, encompass tryptase α (encoded by TPSAB1 in humans), tryptase β (encoded by TPSAB1 and TPSB2 in humans), tryptase δ (encoded by TPSD1 in humans), tryptase γ (encoded by TPSG1 in humans), and tryptase ε (encoded by PRSS22 in humans).[12–15] Tryptase α, β, and γ proteins are soluble, while tryptase ε protein is membrane-anchored. Tryptase β and γ are active serine proteases and exhibit distinct specificities. Tryptase α and δ proteins are mainly inactive proteases due to residue variations at critical positions compared to typical active serine proteases (low activity, limited substrates, consistent with Table 1). Tryptase β is abundant in mast cells and can also be found in basophils.[16] Human tryptase β, generated by the TPSAB1 and TPSB2 loci, exists in three subtypes: β1, β2, and β3, all of which are known as predominantly active tryptases.[17] The specific cleavage sites, substrates, and corresponding potential small molecule inhibitors[18] for these tryptase isoforms remain incompletely elucidated.

Physiologically,[19] tryptases have diverse biological roles during revolution, with significant variations among the isoforms α, β, δ, γ, and ε. Both α-tryptase and β-tryptase are primarily secreted forms found in mast cell granules, playing crucial roles in immune responses, inflammation modulation, and tissue repair. These isoforms contribute to extracellular matrix remodeling and host defense by activating protein

[1]Department of Pancreatic Cancer, Tianjin Medical University Cancer Institute and Hospital, National Clinical Research Center for Cancer, Tianjin's Clinical Research Center for Cancer, Tianjin Key Laboratory of Digestive Cancer, Key Laboratory of Cancer Prevention and Therapy, Tianjin 300060, China
[2]Department of Pharmacy, Tianjin Medical University Cancer Institute and Hospital, National Clinical Research Center for Cancer, Key Laboratory of Cancer Prevention and Therapy, Tianjin's Clinical Research Center for Cancer, Tianjin 300060, China
[3]Department of Bone and Soft Tissue Tumors, Tianjin Medical University Cancer Institute and Hospital, National Clinical Research Center for Cancer, Key Laboratory of Cancer Prevention and Therapy, Tianjin's Clinical Research Center for Cancer, Tianjin 300060, China
[4]Tianjin Key Laboratory of Technologies Enabling Development of Clinical Therapeutics and Diagnostics, The Province and Ministry Co-sponsored Collaborative Innovation Center for Medical Epigenetics, School of Pharmacy, Tianjin Medical University, Tianjin 300070, China
[5]These authors contributed equally
[6]Lead contact
*Correspondence: yingma_maying@hotmail.com (Y.M.), mengshuai2011@126.com (S.M.), haojihui@tjmuch.com (J.H.)
https://doi.org/10.1016/j.isci.2024.110739

Table 1. Isoforms of tryptase family members in human

Isoform	Gene Name	Identifier	Predicted EC Number	Confidence Level
α	TPSAB1	Tryptase α	EC:3.4.21.59	High
β	TPSB2	Tryptase β	EC:3.4.21.59	High
δ	TPSD1	Tryptase δ	EC:3.4.21.59	High
γ	TPSG1	Tryptase γ	EC:3.4.21.106	Low

targets through the cleavage of cell surface receptors or secreted proteins. γ-Tryptase, which is membrane-anchored, helps regulate the local mast cell environment and modulate cell signaling pathways, maintaining structural integrity and facilitating cell interactions. On the other hand, δ-tryptase lacks significant biological activity due to the absence of essential substrate-binding residues and is considered an evolutionary remnant. Information on ε-tryptase is limited, but it is presumed to regulate local tissue environments and immune responses, similar to other tryptases.

Pathologically,[19,20] α and β-tryptases are heavily implicated in allergic reactions and inflammatory diseases, with elevated levels often observed in conditions such as anaphylaxis and mastocytosis. They contribute to disease symptoms through the degradation of extracellular matrix components and the activation of other proteases. α/β-tryptase heterotetramers exhibit unique substrate specificities and stability, playing roles in conditions like hereditary alpha tryptasemia (HaT), which involves excessive mast cell degranulation. γ-tryptase is involved in chronic inflammatory diseases and potentially cancer metastasis by modulating the tumor microenvironment and promoting angiogenesis due to its membrane-bound nature. Although δ-tryptase is inactive enzymatically, its gene presence might indicate a regulatory or structural genomic role, though its impact on pathology remains speculative. ε-tryptase's pathological functions are not well-documented but are likely related to abnormal mast cell activation and extracellular matrix degradation, contributing to disease mechanisms. The varied activities of these isoforms underline the complexity of mast cell functions and highlight the potential for targeted therapeutic interventions in mast cell-related diseases.

Full-length, pro-tryptase β undergoes processing in two proteolytic steps. First, self-catalytic intermolecular cleavage occurs at R-3, particularly at acidic pH and in the presence of polyanions, such as heparin or heparan sulfate. Subsequently, the remaining pro-dipeptide is removed, possibly by dipeptidylpeptidase I. The subunits of the tryptase β tetramer are held together by hydrophobic and polar interactions between the subunits and stabilized by polyanions, especially heparin and heparan sulfate. Mature, enzymatically active tryptase β is stored as a tetramer complexed with heparin in the secretory granules of mast cells.[21] The active sites of each subunit face the central pore of the tetramer, which measures approximately 50 × 30 Å, limiting access of inhibitors to the active sites.[22,23] Exemplary substrates for tryptase β include, but are not limited to, PAR2, C3, fibrinogen, fibronectin, and kininogen.[15]

Currently, the crystal structures of tryptases δ, γ, and ε have not been reported, and their specific enzymatic functions, impact on downstream pathways, and corresponding pathophysiological processes are eagerly awaiting elucidation. In recent years, with breakthroughs in protein structure prediction by AI algorithms such as AlphaFold2,[24,25] it has become possible to obtain high-quality protein and complex structures through computational methods. However, the majority of current AI algorithms rely on training and learning from known protein structures and gene evolutionary relationships, primarily obtained from multiple sequence alignments (MSAs) of existing gene sequences.[26,27] Therefore, the practical prediction accuracy of these AI algorithms often depends on the quality of the target protein's MSA. Yang Zhang's group, collaborating and leading the field,[28,29] has developed two new algorithms to improve the accuracy of protein-protein interaction structure prediction. First, they developed DeepMSA2,[29] which utilizes recursive dynamic programming and hidden Markov model algorithms to rapidly extract high-quality MSA data from massive genomic and metagenomic sequence libraries, creating high-quality deep monomer MSAs. Then, monomer MSAs are paired based on species annotation to construct oligomeric MSAs. Finally, the newly developed DMFold algorithm is used to construct the three-dimensional structure of protein complexes.[30] Their results have shown that DMFold/DeepMSA2 outperforms algorithms such as AlphaFold2 in the prediction accuracy of protein complexes, particularly in the prediction of antibody-antigen complex structures. Therefore, in this study, we employ the aforementioned algorithms for precise prediction of the structures of the tryptase isoforms, and based on this, we utilize methods such as molecular docking to search for potential small molecule inhibitors of these enzymes.

RESULTS

Structural predictions for tryptases α, β, δ, γ, and ε

Since structural predictions and all functional annotations are derived from MSAs for both monomers and multimers, high-quality MSAs are essential to whole prediction. Deep MSA is produced by whole-genome and metagenome sequence database for monomers and is evaluated by calculated score for pairing sequences of multimers, which bring reliable results to this research. We employed the DMFold algorithm to predict the three-dimensional structures of the monomeric forms of tryptases α, β, δ, γ, and ε. For each protease isoform, we selected the top-scoring structure as the adopted model, using the predicted local distance difference test (pLDDT) score,[31] which ranges from 0 to 1, with values closer to 1 indicating higher confidence in the predicted structure's accuracy. As expected, the α and β isoforms, with available crystal structures, exhibited high prediction scores greater than or equal 0.92. Notably, despite lacking experimental structures, the δ, γ, and ε

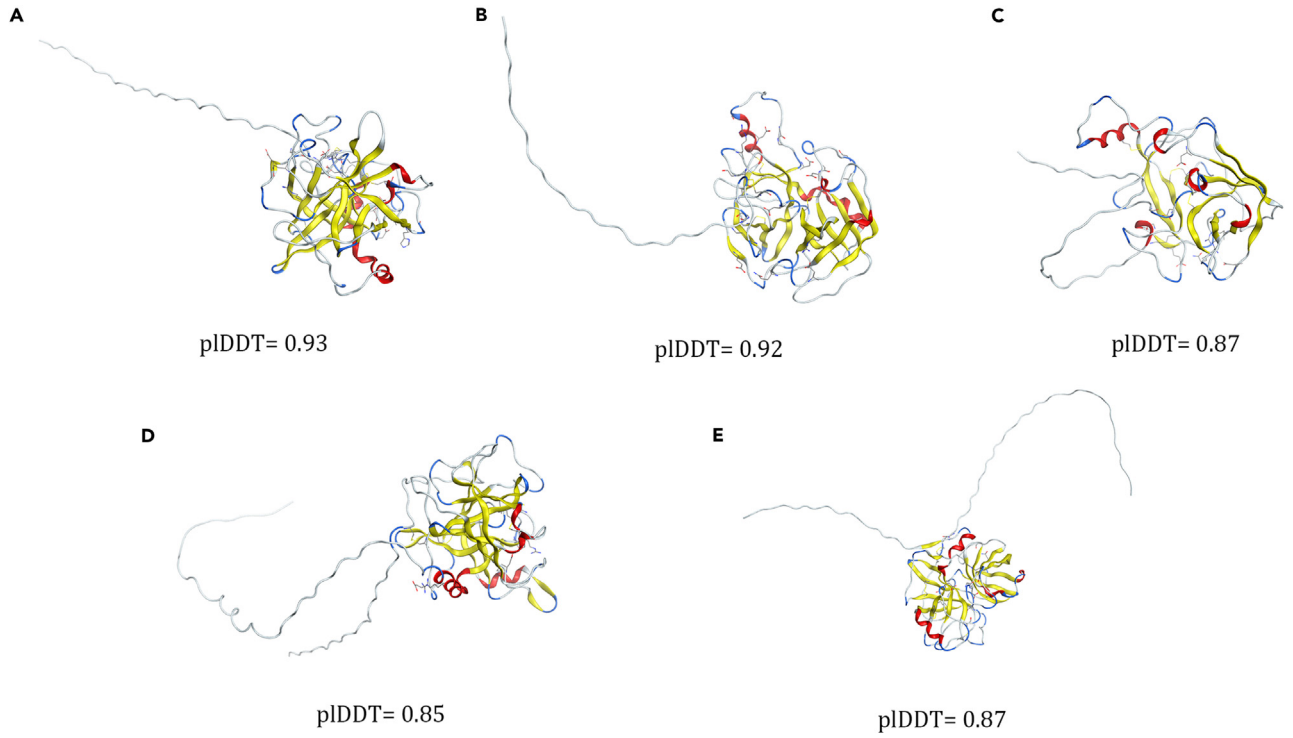

Figure 1. Structural prediction models of tryptases isoforms

(A) Predicted structure of tryptase α.

(B) Predicted structure of tryptase β.

(C) Predicted structure of tryptase δ.

(D) Predicted structure of tryptase γ.

(E) Predicted structure of tryptase ε. Each structure displayed in this figure is selected with the highest predicted score using pLDDT standard for monomer.

isoforms also achieved reasonably high prediction scores above 0.80, attesting to the reliability of the DMFold algorithm in generating accurate structural models (Figure 1). Besides, prediction models of tryptase isoforms that have non-maximum score are displayed in the Figure S1.

Ligand binding site prediction

Based on the high-accuracy models generated by DMFold and the COFACTOR2 algorithm, which integrates structural, sequence, and protein-protein interaction information, we performed local and global structural matching against the BioLiP2 functional site database to identify functional sites and homologs, thereby generating corresponding functional annotations. The ligand binding site prediction provides various scoring metrics representing different dimensions: $Cscore^{LB}$ represents the confidence score of the predicted binding site, ranging from 0 to 1, with higher values indicating more reliable predictions; BS-score reflects the local similarity between the template (homologous protein) binding site and the predicted binding site, with values greater than 1 suggesting significant local matches; TM-score measures the global structural similarity between the template and the predicted protein; $RMSD^{a}$ is the root-mean-square deviation of aligned residues from the structural alignment by TM-align[32]; $IDEN^{a}$ represents the percentage of sequence identity within the structurally aligned regions; Cov denotes the coverage of the global structural alignment, calculated as the number of aligned residues divided by the query protein length.

Using $Cscore^{LB}$ as the primary sorting criterion, the top 10 predicted homologous proteins and their corresponding binding sites were listed for each protease isoform. By superimposing these 10 predictions, we observed that most of the predicted binding sites clustered within a proximal region on the protein structure, suggesting that this area possesses favorable spatial constraints and binding free energies, supporting the inference of the binding site location on the predicted protein structure. Predicted ligand binding sites showed in Tables S1–S5.

Gene ontology prediction (predicted molecular function , biological process , cellular component)

Given the known amino acid sequences of the protease isoforms, we performed annotations for biological processes, molecular functions, and cellular components through sequence alignment against the UniProt-GOA database. The Cscore represents the confidence score for

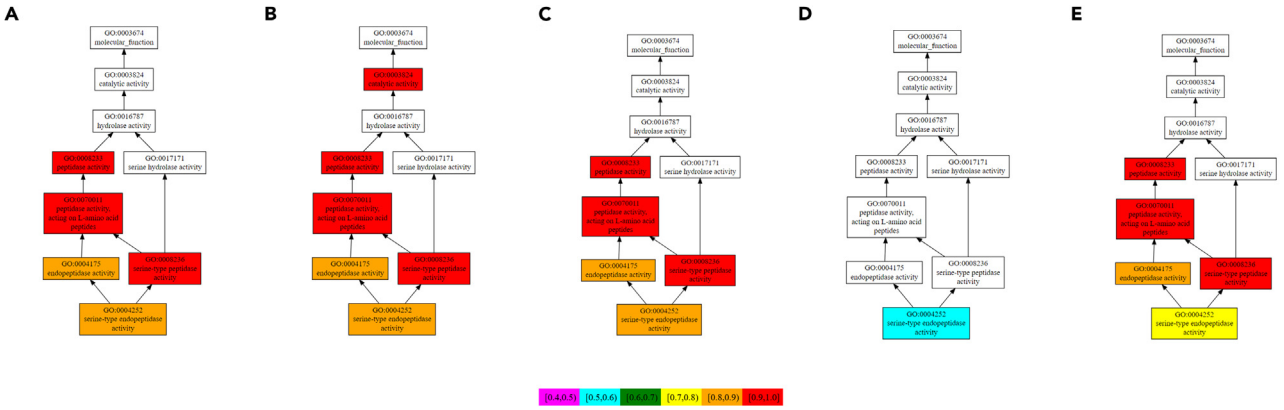

Figure 2. Predicted molecular function of tryptases isoforms

(A) Predicted functional activities of tryptase α.

(B) Predicted functional activities of tryptase β.

(C) Predicted functional activities of tryptase δ.

(D) Predicted functional activities of tryptase γ.

(E) Predicted functional activities of tryptase ε. Confidently score represented by different colors filled in the box, range between 0–1, where a higher value indicates closer to real specific enzyme activities.

each gene ontology term, ranging from 0 to 1, with higher values indicating greater confidence. Additionally, color coding is used to distinguish the more significant terms. As shown in Figure 2, for tryptases α, β, δ, γ, and ε, the primary molecular function (MF) is serine-type peptidase activity (confidence interval 0.9–1), specifically serine-type endopeptidase activity (confidence interval 0.8–0.9). The main biological process (BP) is metabolism (confidence interval 0.8–0.9), particularly protein catabolic process (confidence interval 0.7–0.8). All three isoforms are predicted to be localized intracellularly (CC). For tryptase γ, the gene ontology predictions are less robust, possibly due to its potential extracellular localization (confidence interval 0.8–0.9). As for tryptase ε, its MF and BP predictions align with the first three isoforms, but its cellular component (CC) predictions suggest both intracellular (confidence interval 0.8–0.9) and extracellular (confidence interval 0.5–0.6) localizations. The predicted results of BP and CC are shown in Figure S2.

Enzyme commission number prediction

The enzyme commission (EC) number is a numerical classification scheme based on the chemical reactions catalyzed by enzymes, where each EC number corresponds to a specific enzymatic reaction. Different protein folds may catalyze the same reaction, leading to non-homologous isofunctional enzymes that are assigned the same EC number. Using COFACTOR2 for enzyme classification, our predictions indicate that tryptases α, β, δ, γ, and ε belong to the EC class 3.4.21, serine endopeptidases. However, the specific catalytic functions of each isoform may differ. For instance, tryptases α, β, and γ are predicted to be functionally similar to chymotrypsin (3.4.21.1), pancreatic elastase (3.4.21.36), pancreatic elastase-II (3.4.21.71), and kallikrein (3.4.21.34), while tryptase γ may possess coagulation factor XIa activity. Additionally, tryptase δ, apart from exhibiting tryptase (3.4.21.59) and pancreatic elastase (3.4.21.36) activities, may also possess complement factor D (3.4.21.46) activity. Tryptase ε, in addition to trypsin-like functions, may exhibit enteropeptidase (3.4.21.9) activity. All EC number results predicted by COFACTOR2 are shown in Table S6.

Furthermore, we employed CLEAN,[33] an enzyme activity prediction tool, to predict the enzymatic functions. This tool outperforms others in terms of accuracy, reliability, and sensitivity. EC numbers of different tryptase isoforms predicted by CLEAN are listed in Table 1. Under each isoform, there are minor differences of the predicted putative endogenous substrates based on computational modeling and analysis. Given the higher accuracy and reliability of this analysis, its reference value is more substantial. Tryptases α, β, and δ are functionally classified as trypsin-like enzymes, while tryptases γ and ε are assigned to the broader category of proteases with slightly lower confidence scores. Nonetheless, all isoforms belong to the serine endopeptidase class, consistent with the previous results.

Prediction of small molecule substrates for enzymes

Next, we utilized a deep learning model "ESP" for predicting enzyme-substrate pairs[34] to predict small molecule substrates for different enzyme isoforms. This algorithm achieves over 91% accuracy on test data. We screened 1,126 small molecules, with prediction scores ranging from 0 to 1, where scores above 0.7 are considered more reliable. In our results, we list those small molecule substrates with scores above 0.75.

The results, summarized in Table 2, indicate that tryptase α exhibits catalytic activity toward chlorides; tryptases β, δ, γ, and ε all show catalytic activity toward phenolic compounds. Specifically, tryptase β acts on cyanides, tryptase δ on formyl-CoA, while tryptase ε catalyzes cyanides, naphthoquinones, and 4-nitrophenol.

Table 2. Isoforms of tryptases and substrates

Protease Isoform	Substrates	Score
Tryptase α	chloride	0.756
Tryptase β	phenols	0.960
	cyanate	0.888
Tryptase δ	phenols	0.939
	formyl-CoA(4-)	0.787
Tryptase γ	phenols	0.925
Tryptase ε	phenols	0.946
	cyanate	0.865
	ubiquiones	0.822
	4-nitropheolate	0.817

Virtual screening of small molecule enzyme inhibitors

We employed the molecular modeling software Schrodinger to perform virtual screening of small molecule inhibitors against different tryptase isoforms. Tryptases α and β are soluble proteases with 93–99% sequence homology.[35] The crystal structures of tryptase α (PDB: 1LTO) and tryptase β (PDB: 1A0L) and their alignment reveal high similarity between them (Figure 3). Tryptase α is inertia in proteolysis, and this structure does not require heparin binding for stability. Therefore, we selected the tryptase β protein (PDB: 1A0L) as the target for screening small molecule inhibitors.

The small molecule (2S)-3-(4-carbamimidoylphenyl)-2-hydroxypropanoic acid is bound to tryptase β (Figure S3), forming hydrogen bonds with the active site residues Asp189, Gly219, and the carbonyl and hydroxyl oxygens form hydrogen bonds with Ser195. The molecule forms a covalent bond with the target. We centered the docking grid on this region (Figure S4). The Maybridge small molecule screening library containing over 60,000 compounds with over 300 distinct heterocyclic systems, covering 87% of 400,000 theoretical pharmacophores, was selected to balance chemical space coverage and the number of fragments to screen, as recognized by the experts in the field.

Screening results (Figures 4 and S5) showed 63 compounds with absolute docking scores above 7.5. These compounds form hydrogen bond networks or π-π interactions with active site residues: Asp189 (hydrogen bonding); Ser190 (hydrogen bonding); Gly219 (hydrogen bonding); Ser195 (hydrogen bonding); Gly216 (hydrogen bonding); Gln192 (hydrogen bonding); His57 (π-π interaction). Twelve compounds scored higher than the existing ligand (2S)-3-(4-carbamimidoylphenyl)-2-hydroxypropanoic acid (docking score = −8.238) (Figures 5A and S5;

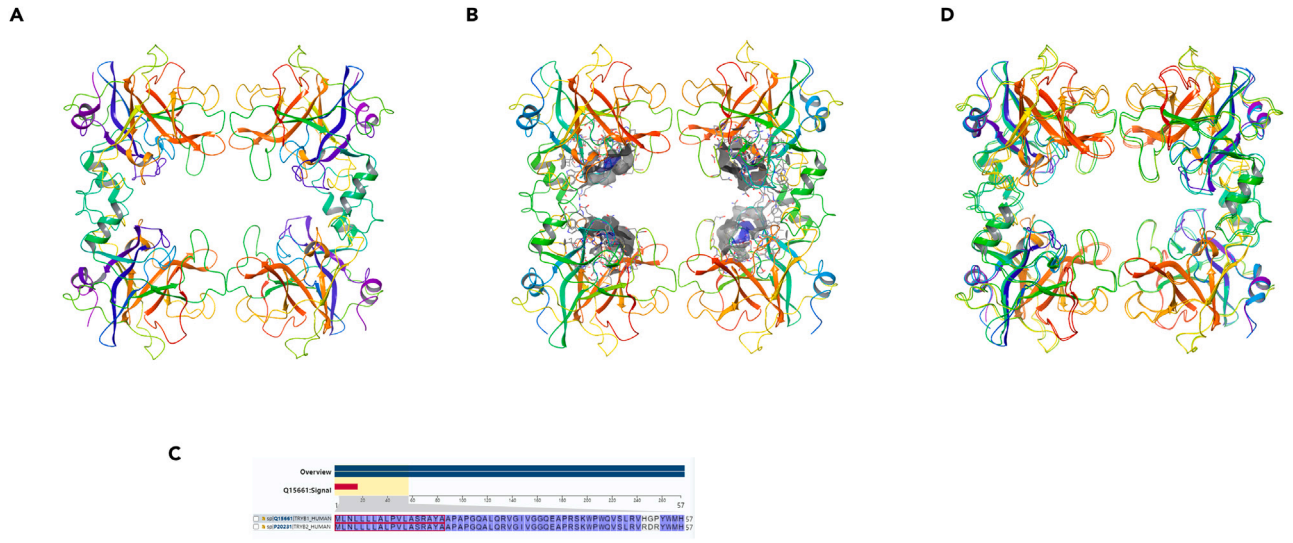

Figure 3. Crystal structures of tryptases α (PDB: 1LTO) and β (PDB: 1A0L), and alignment of them

(A) Crystal structure of tryptase α.

(B) Crystal structure of tryptase β.

(C) Alignment of sequences of two tryptases.

(D) Alignment of structures of tryptases α and β.

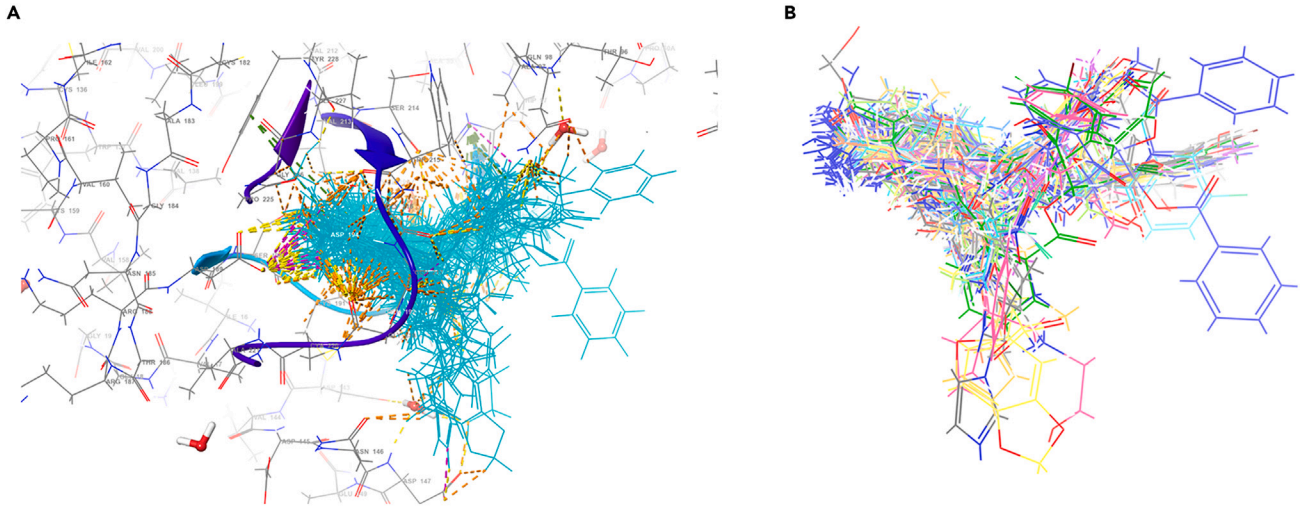

Figure 4. Generalized binding sites for small molecules docking to tryptase β

(A) Generalized binding sites for compounds from Maybridge library docking to tryptase β, including hydrogen bonding with ASP189, SER190, GLY219, Ser195, GLY216, GLN192, and π-π interaction with HIP57.

(B) Alignment of all selected compounds, which scoring range from −7.5 to 9.395.

Table S7). Among them, 3-chloro-4-methylbenzimidamide has a docking score of −9.395, and its interaction diagram is shown (Figures 5B and 5C).

Next, we docked these 63 compounds against tryptases δ, γ and ε to assess their selectivity. We performed molecular docking using the tryptases δ, γ, and ε structures built by the DMFold algorithm, as their active sites are unknown. The SiteMap algorithm,[36,37] which combines geometric, energetic, and chemical properties to predict binding sites with 86% accuracy on a set of 538 protein-ligand complexes from the PDBbind database, was used to identify and score potential binding pockets (Figure S6; Table S8).

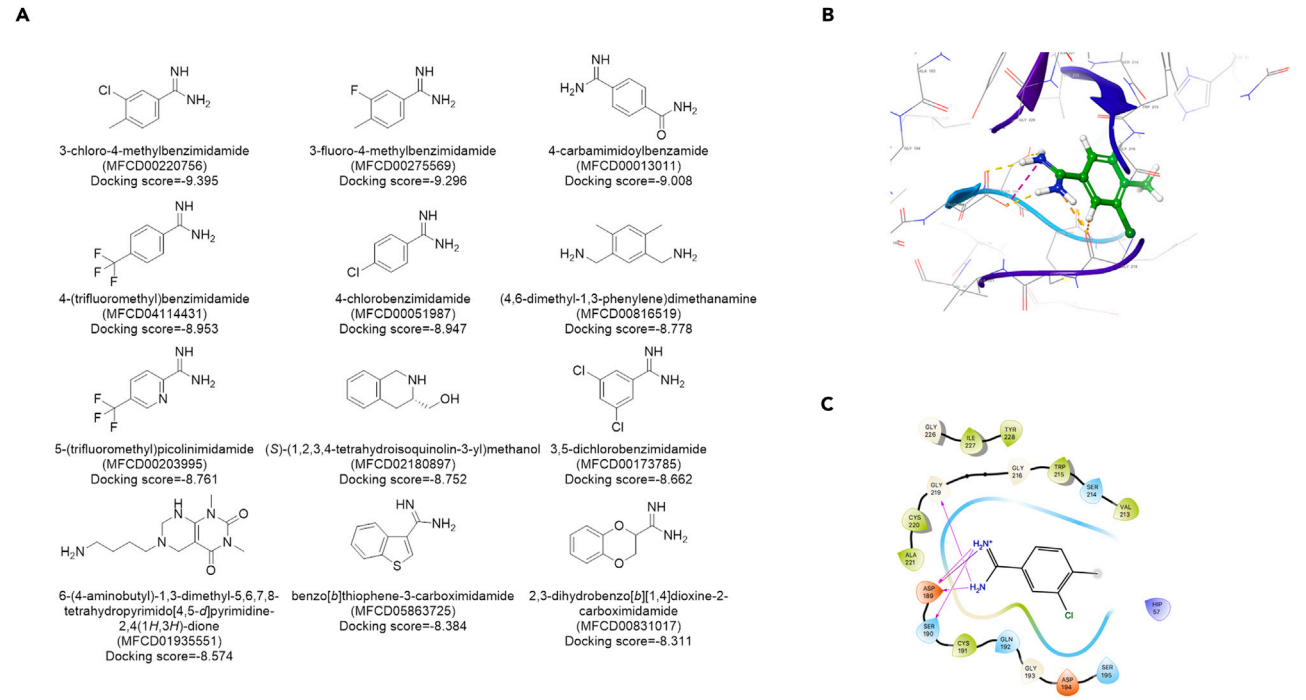

Figure 5. Results of compounds docking to tryptase β

(A) Structures of top 12 score compounds docking to tryptase β.

(B) Small molecule MFCD00220756 interact with tryptase β in 3D perspective.

(C) MFCD00220756 interacts with tryptase β in 2D perspective.

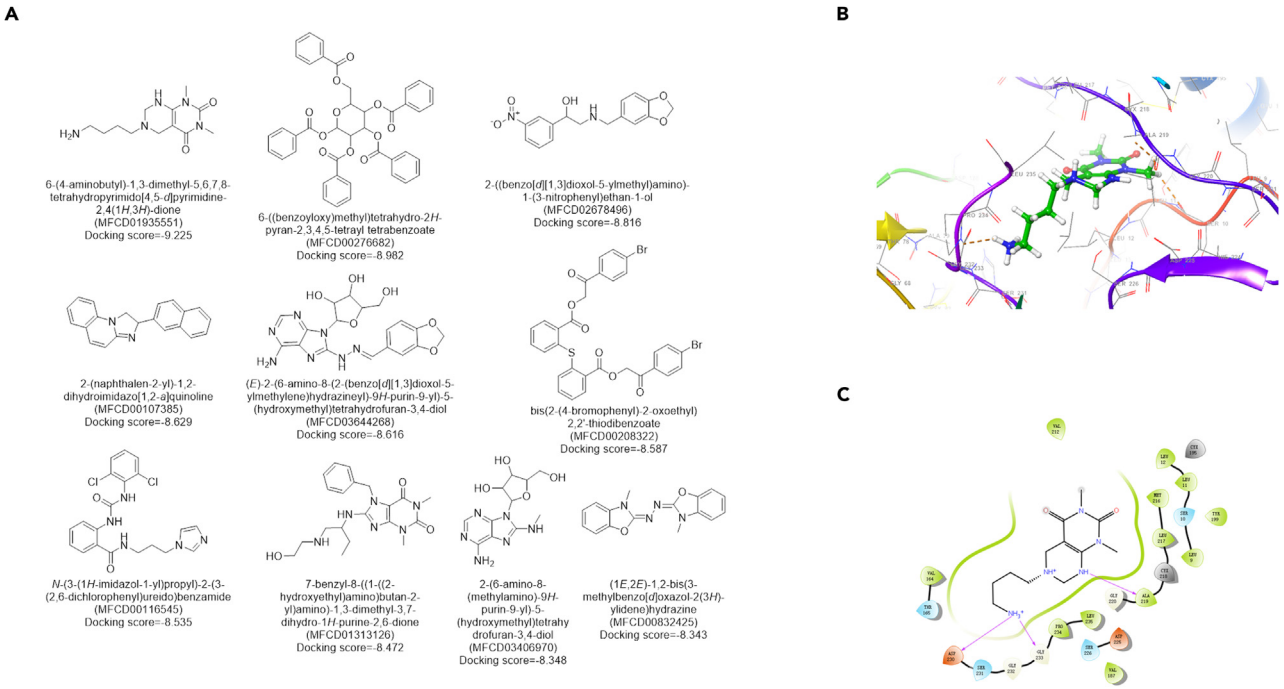

Figure 6. Results of compounds docking to tryptase δ

(A) Structures of top 10 score compounds docking to tryptase δ.

(B) Small molecule MFCD01935551 interact with tryptase β in 3D perspective.

(C) MFCD01935551 interacts with tryptase β in 2D perspective.

Docking results of candidate inhibitors with tryptase δ are shown in Figure 6; 10 compounds had absolute docking scores above 8.2. Except for MFCD01935551, the others differed from the high-affinity compounds for tryptase β. MFCD01935551 forms hydrogen bonds with Asp230, Gly233, and Ala219 of tryptase δ.

Candidate inhibitors binding to tryptase γ are shown in Figure 7; 3 compounds had absolute docking scores above 8.2. MFCD02678496 formed a cation-π interaction with His78, hydrogen bonds with Ser241 and Gly118, and a salt bridge with Asp125. Interestingly, it also bound tryptase δ (docking score −8.816).

Tryptase ε generally showed weaker binding to these candidate inhibitors, with the strongest being −7.655, as shown in Figure S7.

The compound MFCD00220756 with the highest affinity for tryptase β only had a docking score of −6.639 for tryptase δ, and −7.469 and −7.425 for tryptases γ and ε, respectively, suggesting the selectivity of MFCD00220756 for tryptase β.

Experimental validation of small molecule enzyme inhibitors

To validate our virtual screening results, we experimentally evaluated three available compounds (Table S7) for their ability to inhibit tryptase β-mediated proliferation of human pancreatic stellate cells (HPSCs) using an assay generated in our platform.[5]

Compound 22978-61-6 demonstrated a potent, dose-dependent inhibition of HPSC proliferation (Figure 8A). At 1 μM concentration, it significantly reduced proliferation to levels comparable with serum-free medium (SFM) conditions ($p < 0.01$). This inhibitory effect was further presented by CFSE (carboxyfluorescein succinimidyl ester) dilution assay (Figure 8B), where HPSCs treated with 1 μM of 22978-61-6 retained more CFSE fluorescence compared to untreated cells, indicating reduced cell division, and effective inhibition of the tryptase inhibitor.

In contrast, compounds 59855-11-7 and 18881-17-9 did not exhibit significant inhibition of HPSC proliferation across the tested concentration range (0.03–1 μM) (Figure 8A).

As expected, HPSCs cultured in RPMI1640 plus fetal bovine serum (FBS) showed significantly higher proliferation rates compared to those in SFM ($p < 0.001$), validating the assay's sensitivity to proliferative stimuli.

These experimental findings provide strong support for our virtual screening approach, particularly in identifying compound 22978-61-6 as a potent tryptase β inhibitor. The results underscore the potential of our computational method for discovering tryptase β inhibitors and highlight the importance of experimental validation in drug discovery pipelines.

DISCUSSION

Our study demonstrates the power of integrating computational predictions with experimental validation in the search for tryptase inhibitors, yielding several significant insights. The successful identification of compound 22978-61-6 as a potent inhibitor of tryptase β-mediated HPSC

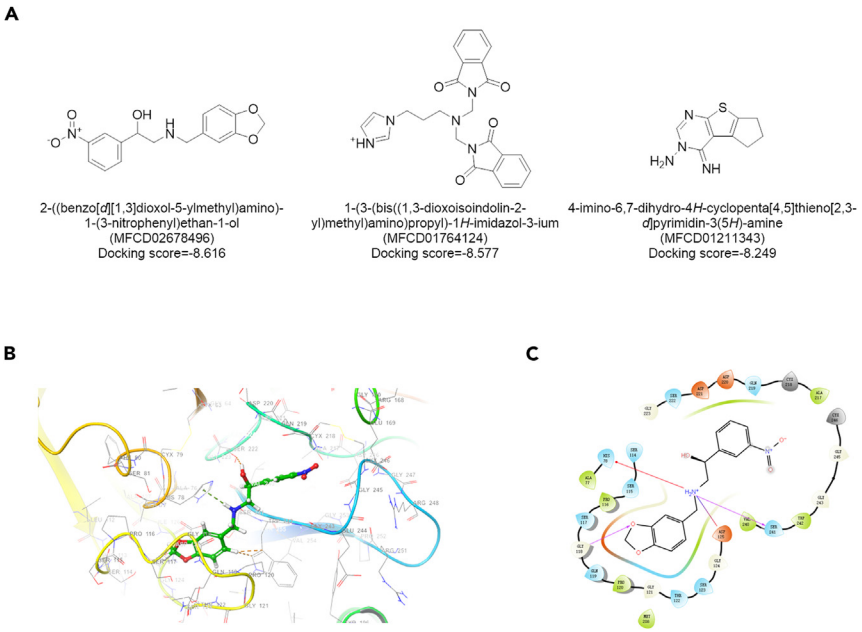

Figure 7. Results of compounds docking to tryptase γ

(A) Structures of top 3 score compounds docking to tryptase γ.

(B) Small molecule MFCD026784961interact with tryptase γ in 3D perspective.

(C) MFCD02678496 interact with tryptase γ in 2D perspective.

proliferation validates our virtual screening approach, underscoring the potential of *in silico* methods to accelerate drug discovery processes, particularly for challenging targets like tryptase β. The differential effects observed among the three tested compounds provide valuable insights into structure-activity relationships, with the unique structural features of 22978-61-6 potentially guiding future optimization efforts and the design of more potent and selective tryptase β inhibitors. Furthermore, the inhibition of HPSC proliferation by 22978-61-6 suggests a potential role for tryptase β in pancreatic fibrosis, a hallmark of chronic pancreatitis and pancreatic cancer, opening new avenues for investigating the role of mast cells and tryptase in pancreatic pathologies. However, it's important to note that while our approach successfully identified one potent inhibitor, the lack of activity in the other two compounds emphasizes the importance of experimental validation and highlights the current limitations of computational methods, underscoring the need for continued refinement of predictive algorithms. This balanced perspective on our findings not only validates our approach but also acknowledges areas for improvement, setting the stage for future advancements in treating mast cell-related disorders, including anaphylaxis,[38] such as airway hyperreactivity,[39] food allergy,[40] or tissue damage caused by environmental hazards or animal venoms[41]; chronic inflammatory diseases[42,43]; and cancers, such as pancreatic cancer,[5,7] mastocytosis,[44] tumor-associated hydrocephalus, Li et al.[18]

Taken together, we employed Schrodinger to screen for small molecule inhibitors against tryptase β, and then performed virtual docking of these inhibitors against other tryptase isoforms. We found that the screened small molecule inhibitors exhibited relatively high selectivity for tryptase β, providing a theoretical basis for the further development of tryptase inhibitors.

Our study highlights the potential of computational methods, such as DMFold and DeepMSA2, in predicting protein structures and facilitating the discovery of selective inhibitors for therapeutic targets. The identified compounds serve as promising starting points for the development of selective tryptase inhibitors, which may have applications in the treatment of various diseases associated with tryptase activity, such as asthma, inflammatory conditions, and cancer.

In conclusion, our study demonstrates the power of integrating advanced computational methods, such as DMFold, DeepMSA2, and molecular docking, in the discovery of selective small molecule inhibitors for therapeutic targets. The identified compounds provide a solid foundation for the development of selective tryptase inhibitors, which may have broad implications in the treatment of various diseases. Further experimental validation and optimization of these compounds are warranted to translate these findings into clinical applications.

Limitations of the study

Our study has several limitations that should be acknowledged. First, the computational protein structure predictions, while highly accurate, have not been experimentally validated through crystallographic or other structural biology techniques. Further experimental work will be necessary to confirm the predicted structures and active site configurations of the tryptase isoforms. Additionally, the computational docking and virtual screening approaches used to identify potential substrates and inhibitors provide promising leads, but the actual biochemical activities and selectivity of the top compounds will need to be verified through selectivity profiling. Finally, this study was focused solely

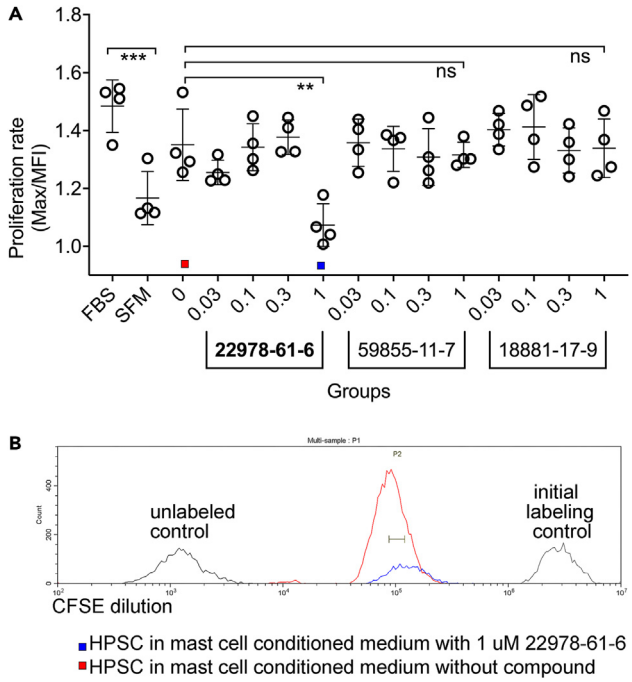

Figure 8. Experimental validation of virtually screened tryptase β inhibitors

(A) Proliferation rate of human pancreatic stellate cells (HPSCs) under various conditions. Cells were cultured in RPMI1640 plus fetal bovine serum (FBS), serum-free RPMI1640 medium (SFM), or mast cell conditioned medium with different concentrations (0–1 μM) of compounds 22978-61-6, 59855-11-7, and 18881-17-9. Proliferation rate is expressed as Max/MFI (maximum/median fluorescence intensity). Each point represents an individual replicate; error bars show mean ± SD. $p < 0.0001$ is for all groups as determined by use of a one-way ANOVA, followed by Tukey's multiple comparison test. Statistical significance: ***$p < 0.001$, **$p < 0.01$, ns: not significant.

(B) CFSE dilution assay showing cell proliferation. The histogram displays CFSE fluorescence intensity for unlabeled control, initial labeling control, HPSCs in mast cell conditioned medium without compound (red), and HPSCs treated with 1 μM of compound 22978-61-6 (blue). Higher CFSE retention indicates reduced cell division.

on the structural and functional predictions of the tryptase family; following *in vitro* and *in vivo* studies are necessary to confirm the binding affinity, selectivity, and efficacy of the identified compounds. The next critical step will be to evaluate the biological relevance and translational potential of these findings in appropriate *in vivo* animal models of inflammatory diseases and cancer.[45] Especially, the potential off-target effects and toxicity of these compounds should be carefully evaluated before considering them for clinical applications.[46] Despite these limitations, we believe the integrative computational framework developed here represents a significant step forward in characterizing this important family of proteases and identifying selective therapeutic candidates worthy of further investigation.

RESOURCE AVAILABILITY

Lead contact

Further information and requests for resources and reagents should be directed to and will be fulfilled by the Lead Contact, Ying Ma (yingma_maying@hotmail.com or yingma@tmu.edu.cn), twitter handle: yingma_maying.

Materials availability

This study did not generate new unique reagents.

Data and code availability

- The protein sequences that support the findings of this study are openly available in the Uniprot database.
- All original code is publicly available. DOIs are listed in the key resources table.
- Any additional information required to reanalyze the data reported in this paper is available from the lead contact upon request.

ACKNOWLEDGMENTS

The authors thank their team members for discussion and cooperation. While using ChatGPT and Claude-3 for language editing, the authors carefully reviewed and validated the words and sentences generated by ChatGPT or Claude-3 before including them in the article.

This research was funded by The National Natural Science Foundation of China (NSFC) grants, grant number 82072691 and 82272767 to Y.M.

AUTHOR CONTRIBUTIONS

Conceptualization: Y.M., B.L., and S.M.; methodology: B.L. and S.M.; validation: B.L. and S.M.; formal analysis: B.L. and S.M.; investigation: Y.M., B.L., X.Z., Y.L., X.L., J.Z., Y.W., L.W., and S.M.; data curation: B.L. and S.M.; writing—original draft: B.L. and S.M.; writing—review, editing, and revision: Y.M., B.L., and X.Z.; visualization: B.L. and S.M.; supervision: Y.M., J.Z., and J.H.; project administration/oversight: Y.M. and S.M.; funding acquisition: Y.M.

DECLARATION OF INTERESTS

The authors have declared that they have no conflicts of interest.

STAR★METHODS

Detailed methods are provided in the online version of this paper and include the following:

- KEY RESOURCES TABLE
- EXPERIMENTAL MODEL AND STUDY PARTICIPANT DETAILS
- METHOD DETAILS
  - Computational analysis
  - Experimental evaluation of tryptase inhibitor efficacy via cell proliferation analysis
- QUANTIFICATION AND STATISTICAL ANALYSIS

SUPPLEMENTAL INFORMATION

Supplemental information can be found online at https://doi.org/10.1016/j.isci.2024.110739.

Received: May 3, 2024
Revised: July 13, 2024
Accepted: August 12, 2024
Published: August 21, 2024

REFERENCES

1. Plum, T., Binzberger, R., Thiele, R., Shang, F., Postrach, D., Fung, C., Fortea, M., Stakenborg, N., Wang, Z., Tappe-Theodor, A., et al. (2023). Mast cells link immune sensing to antigen-avoidance behaviour. Nature *620*, 634–642. https://doi.org/10.1038/s41586-023-06188-0.
2. Starkl, P., Watzenboeck, M.L., Popov, L.M., Zahalka, S., Hladik, A., Lakovits, K., Radhouani, M., Haschemi, A., Marichal, T., Reber, L.L., et al. (2020). IgE Effector Mechanisms, in Concert with Mast Cells, Contribute to Acquired Host Defense against Staphylococcusaureus. Immunity *53*, 793–804.e9. https://doi.org/10.1016/j.immuni.2020.08.002.
3. Serhan, N., Basso, L., Sibilano, R., Petitfils, C., Meixiong, J., Bonnart, C., Reber, L.L., Marichal, T., Starkl, P., Cenac, N., et al. (2019). House dust mites activate nociceptor-mast cell clusters to drive type 2 skin inflammation. Nat. Immunol. *20*, 1435–1443. https://doi.org/10.1038/s41590-019-0493-z.
4. Mencarelli, A., Bist, P., Choi, H.W., Khameneh, H.J., Mortellaro, A., and Abraham, S.N. (2024). Anaphylactic degranulation by mast cells requires the mobilization of inflammasome components. Nat. Immunol. *25*, 693–702. https://doi.org/10.1038/s41590-024-01788-y.
5. Ma, Y., Hwang, R.F., Logsdon, C.D., and Ullrich, S.E. (2013). Dynamic mast cell-stromal cell interactions promote growth of pancreatic cancer. Cancer Res. *73*, 3927–3937. https://doi.org/10.1158/0008-5472.CAN-12-4479.
6. Chacòn-Salinas, R., Chen, L., Chavez-Blanco, A.D., Limon-Flores, A.Y., Ma, Y., and Ullrich, S.E. (2014). An essential role for platelet-activating factor in activating mast cell migration following ultraviolet irradiation. J. Leukocyte Biol. *95*, 139–148. https://doi.org/10.1189/jlb.0811409.
7. Ma, Y., and Ullrich, S.E. (2013). Intratumoral mast cells promote the growth of pancreatic cancer. OncoImmunology *2*, e25964. https://doi.org/10.4161/onci.25964.
8. Chang, D.Z., Ma, Y., Ji, B., Wang, H., Deng, D., Liu, Y., Abbruzzese, J.L., Liu, Y.J., Logsdon, C.D., and Hwu, P. (2011). Mast cells in tumor microenvironment promotes the in vivo growth of pancreatic ductal adenocarcinoma. Clin. Cancer Res. *17*, 7015–7023. https://doi.org/10.1158/1078-0432.CCR-11-0607.
9. He, Y., Wu, S., Yuan, Y., Sun, Y., Ai, Q., Zhou, R., Chai, G., Chen, D., and Hu, H. (2023). Remodeling tumor immunosuppression with molecularly imprinted nanoparticles to enhance immunogenic cell death for cancer immunotherapy. J. Control. Release *362*, 44–57. https://doi.org/10.1016/j.jconrel.2023.08.026.
10. Pereira, B.A., Lister, N.L., Hashimoto, K., Teng, L., Flandes-Iparraguirre, M., Eder, A., Sanchez-Herrero, A., and Niranjan, B.; Melbourne Urological Research Alliance MURAL (2019). Tissue engineered human prostate microtissues reveal key role of mast cell-derived tryptase in potentiating cancer-associated fibroblast (CAF)-induced morphometric transition in vitro. Biomaterials *197*, 72–85. https://doi.org/10.1016/j.biomaterials.2018.12.030.
11. Yang, L., He, H., Guo, X.K., Wang, J., Wang, W., Li, D., Liang, S., Shao, F., Liu, W., and Hu, X. (2024). Intraepithelial mast cells drive gasdermin C-mediated type 2 immunity. Immunity *57*, 1056–1070.e5. https://doi.org/10.1016/j.immuni.2024.03.017.
12. Hallgren, J., and Pejler, G. (2006). Biology of mast cell tryptase. An inflammatory mediator. FEBS J. *273*, 1871–1895. https://doi.org/10.1111/j.1742-4658.2006.05211.x.
13. Sprinzl, B., Greiner, G., Uyanik, G., Arock, M., Haferlach, T., Sperr, W.R., Valent, P., and Hoermann, G. (2021). Genetic Regulation of Tryptase Production and Clinical Impact: Hereditary Alpha Tryptasemia, Mastocytosis and Beyond. Int. J. Mol. Sci. *22*, 2458. https://doi.org/10.3390/ijms22052458.
14. Maaninka, K., Lappalainen, J., and Kovanen, P.T. (2013). Human mast cells arise from a common circulating progenitor. J. Allergy Clin. Immunol. *132*, 463–469.e3. https://doi.org/10.1016/j.jaci.2013.02.011.
15. Fukuoka, Y., and Schwartz, L.B. (2007). Active monomers of human beta-tryptase have expanded substrate specificities. Int. Immunopharmacol. *7*, 1900–1908. https://doi.org/10.1016/j.intimp.2007.07.007.
16. Jogie-Brahim, S., Min, H.K., Fukuoka, Y., Xia, H.Z., and Schwartz, L.B. (2004). Expression of alpha-tryptase and beta-tryptase by human basophils. J. Allergy Clin. Immunol. *113*, 1086–1092. https://doi.org/10.1016/j.jaci.2004.02.032.
17. Payne, V., and Kam, P.C.A. (2004). Mast cell tryptase: a review of its physiology and clinical significance. Anaesthesia *59*, 695–703. https://doi.org/10.1111/j.1365-2044.2004.03757.x.
18. Li, Y., Di, C., Song, S., Zhang, Y., Lu, Y., Liao, J., Lei, B., Zhong, J., Guo, K., Zhang, N., and Su, S. (2023). Choroid plexus mast cells drive tumor-associated hydrocephalus. Cell *186*, 5719–5738.e28. https://doi.org/10.1016/j.cell.2023.11.001.
19. Lyons, J.J., and Yi, T. (2021). Mast cell tryptases in allergic inflammation and immediate hypersensitivity. Curr. Opin. Immunol. *72*, 94–106. https://doi.org/10.1016/j.coi.2021.04.001.

20. O'Connell, M.P., and Lyons, J.J. (2022). Resolving the genetics of human tryptases: implications for health, disease, and clinical use as a biomarker. Curr. Opin. Allergy Clin. Immunol. *22*, 143–152. https://doi.org/10.1097/ACI.0000000000000813.
21. Maun, H.R., Liu, P.S., Franke, Y., Eigenbrot, C., Forrest, W.F., Schwartz, L.B., and Lazarus, R.A. (2018). Dual functionality of beta-tryptase protomers as both proteases and cofactors in the active tetramer. J. Biol. Chem. *293*, 9614–9628. https://doi.org/10.1074/jbc.M117.812016.
22. Sommerhoff, C.P., Bode, W., Pereira, P.J., Stubbs, M.T., Stürzebecher, J., Piechottka, G.P., Matschiner, G., and Bergner, A. (1999). The structure of the human bII-tryptase tetramer: Fo(u)r better or worse. Proc. Natl. Acad. Sci. USA *96*, 10984–10991.
23. Pereira, P.J., Bergner, A., Macedo-Ribeiro, S., Huber, R., Matschiner, G., Fritz, H., Sommerhoff, C.P., and Bode, W. (1998). Human β-tryptase is a ring-like tetramer with active sites facing a central pore. Nature *392*, 306–311.
24. Yang, Z., Zeng, X., Zhao, Y., and Chen, R. (2023). AlphaFold2 and its applications in the fields of biology and medicine. Signal Transduct. Target. Ther. *8*, 115. https://doi.org/10.1038/s41392-023-01381-z.
25. Bryant, P., Pozzati, G., and Elofsson, A. (2022). Improved prediction of protein-protein interactions using AlphaFold2. Nat. Commun. *13*, 1265. https://doi.org/10.1038/s41467-022-28865-w.
26. Varga, J.K., and Schueler-Furman, O. (2023). Who Binds Better? Let Alphafold2 Decide. Angew. Chem. Int. Ed. Engl. *62*, e202303526. https://doi.org/10.1002/anie.202303526.
27. Chowdhury, R., Bouatta, N., Biswas, S., Floristean, C., Kharkar, A., Roy, K., Rochereau, C., Ahdritz, G., Zhang, J., Church, G.M., et al. (2022). Single-sequence protein structure prediction using a language model and deep learning. Nat. Biotechnol. *40*, 1617–1623. https://doi.org/10.1038/s41587-022-01432-w.
28. Zheng, W., Wuyun, Q., Freddolino, P.L., and Zhang, Y. (2023). Integrating deep learning, threading alignments, and a multi-MSA strategy for high-quality protein monomer and complex structure prediction in CASP15. Proteins *91*, 1684–1703. https://doi.org/10.1002/prot.26585.
29. Zheng, W., Wuyun, Q., Li, Y., Zhang, C., Freddolino, P.L., and Zhang, Y. (2024). Improving deep learning protein monomer and complex structure prediction using DeepMSA2 with huge metagenomics data. Nat. Methods *21*, 279–289. https://doi.org/10.1038/s41592-023-02130-4.
30. Wang, L., Liu, Y., Zhong, X., Liu, H., Lu, C., Li, C., and Zhang, H. (2019). DMfold: A Novel Method to Predict RNA Secondary Structure With Pseudoknots Based on Deep Learning and Improved Base Pair Maximization Principle. Front. Genet. *10*, 143. https://doi.org/10.3389/fgene.2019.00143.
31. Mariani, V., Biasini, M., Barbato, A., and Schwede, T. (2013). lDDT: a local superposition-free score for comparing protein structures and models using distance difference tests. Bioinformatics *29*, 2722–2728. https://doi.org/10.1093/bioinformatics/btt473.
32. Zhang, Y., and Skolnick, J. (2005). TM-align: a protein structure alignment algorithm based on the TM-score. Nucleic Acids Res. *33*, 2302–2309. https://doi.org/10.1093/nar/gki524.
33. Yu, T., Cui, H., Li, J.C., Luo, Y., Jiang, G., and Zhao, H. (2023). Enzyme function prediction using contrastive learning. Science *379*, 1358–1363. https://doi.org/10.1126/science.adf2465.
34. Kroll, A., Ranjan, S., Engqvist, M.K.M., and Lercher, M.J. (2023). A general model to predict small molecule substrates of enzymes based on machine and deep learning. Nat. Commun. *14*, 2787. https://doi.org/10.1038/s41467-023-38347-2.
35. Caughey, G.H. (2006). Tryptase genetics and anaphylaxis. J. Allergy Clin. Immunol. *117*, 1411–1414. https://doi.org/10.1016/j.jaci.2006.02.026.
36. Halgren, T. (2007). New method for fast and accurate binding-site identification and analysis. Chem. Biol. Drug Des. *69*, 146–148. https://doi.org/10.1111/j.1747-0285.2007.00483.x.
37. Halgren, T.A. (2009). Identifying and characterizing binding sites and assessing druggability. J. Chem. Inf. Model. *49*, 377–389. https://doi.org/10.1021/ci800324m.
38. Bordon, Y. (2023). Mast cells chill in anaphylaxis. Nat. Rev. Immunol. *23*, 270. https://doi.org/10.1038/s41577-023-00875-9.
39. Su, Y., Xu, J., Zhu, Z., Chin, J., Xu, L., Yu, H., Nudell, V., Dash, B., Moya, E.A., Ye, L., et al. (2024). Brainstem Dbh+ neurons control allergen-induced airway hyperreactivity. Nature *631*, 601–609. https://doi.org/10.1038/s41586-024-07608-5.
40. Florsheim, E.B., Bachtel, N.D., Cullen, J.L., Lima, B.G.C., Godazgar, M., Carvalho, F., Chatain, C.P., Zimmer, M.R., Zhang, C., Gautier, G., et al. (2023). Immune sensing of food allergens promotes avoidance behaviour. Nature *620*, 643–650. https://doi.org/10.1038/s41586-023-06362-4.
41. Link, K., Muhandes, L., Polikarpova, A., Lämmermann, T., Sixt, M., Fässler, R., and Roers, A. (2024). Integrin β1-mediated mast cell immune-surveillance of blood vessel content. J. Allergy Clin. Immunol. *16*. S0091-6749(24)00362-2. https://doi.org/10.1016/j.jaci.2024.03.022.
42. Kotrba, J., and Dudeck, A. (2024). Mast cells: The Janus of type 2 inflammation. Immunity *57*, 1182–1184. https://doi.org/10.1016/j.immuni.2024.05.011.
43. Kolkhir, P., Akdis, C.A., Akdis, M., Bachert, C., Bieber, T., Canonica, G.W., Guttman-Yassky, E., Metz, M., Mullol, J., Palomares, O., et al. (2023). Type 2 chronic inflammatory diseases: targets, therapies and unmet needs. Nat. Rev. Drug Discov. *22*, 743–767. https://doi.org/10.1038/s41573-023-00750-1.
44. Lübke, J., Schwaab, J., Naumann, N., Horny, H.-P., Weiß, C., Metzgeroth, G., Kreil, S., Cross, N.C.P., Sotlar, K., Fabarius, A., et al. (2022). Superior Efficacy of Midostaurin Over Cladribine in Advanced Systemic Mastocytosis: A Registry-Based Analysis. J. Clin. Oncol. *40*, 1783–1794. https://doi.org/10.1200/JCO.21.01849.
45. Maun, H.R., Jackman, J.K., Choy, D.F., Loyet, K.M., Staton, T.L., Jia, G., Dressen, A., Hackney, J.A., Bremer, M., Walters, B.T., et al. (2019). An Allosteric Anti-tryptase Antibody for the Treatment of Mast Cell-Mediated Severe Asthma. Cell *179*, 417–431.e19. https://doi.org/10.1016/j.cell.2019.09.009.
46. Lübke, J., Schwaab, J., Naumann, N., Horny, H.P., Weiss, C., Metzgeroth, G., Kreil, S., Cross, N.C.P., Sotlar, K., Fabarius, A., et al. (2022). Superior Efficacy of Midostaurin Over Cladribine in Advanced Systemic Mastocytosis: A Registry-Based Analysis. J. Clin. Oncol. *40*, 1783–1794. https://doi.org/10.1200/JCO.21.01849.
47. Billesbølle, C.B., de March, C.A., van der Velden, W.J.C., Ma, N., Tewari, J., Del Torrent, C.L., Li, L., Faust, B., Vaidehi, N., Matsunami, H., and Manglik, A. (2023). Structural basis of odorant recognition by a human odorant receptor. Nature *615*, 742–749. https://doi.org/10.1038/s41586-023-05798-y.

STAR★METHODS

KEY RESOURCES TABLE

REAGENT or RESOURCE	SOURCE	IDENTIFIER
Chemicals, peptides, and recombinant proteins		
CFSE (carboxyfluorescein succinimidyl ester)	BioLegend	Cat#423801
Compound (18881-17-9)	Bidepharm	Cat#BD0195-250mg
Compound (59855-11-7)	Bidepharm	Cat#BD5142-1g
Compound (22978-61-6)	MCE	Cat#HY-W296205
Experimental models: cell lines		
HMC-1 (Human mast cell line)	https://doi.org/10.1158/0008-5472.CAN-12-4479	N/A
Human pancreatic stellate cells (HPSCs)	https://doi.org/10.1158/0008-5472.CAN-12-4479	N/A
Deposited data		
Protein sequences	UniProt database	N/A
Software and algorithms		
DMFold	Zhang Lab (https://zhanggroup.org/DMFold/)	https://doi.org/10.1038/s41592-023-02130-4
DeepMSA2	Zhang Lab (https://zhanggroup.org/DeepMSA/)	https://doi.org/10.1038/s41592-023-02130-4
COFACTOR2	Zhang Lab (https://zhanggroup.org/COFACTOR/)	https://doi.org/10.1038/s41592-023-02130-4
CLEAN	Molecule Maker Lab Institute (https://github.com/tttianhao/CLEAN)	https://doi.org/10.1126/science.adf2465
SiteMap	Schrödinger	https://doi.org/10.1021/ci800324m
ESP	DeepMolecules@hhu.de (https://github.com/AlexanderKroll/ESP)	https://doi.org/10.1038/s41467-023-38347-2
CytExpert	Beckman Coulter	N/A
Flow cytometer		
Beckman Coulter Flow Cytometer (21 Detectors, 6 Lasers)	Beckman Coulter	CytoFLEX LX U3-V5-B3-Y5-R3-I2

EXPERIMENTAL MODEL AND STUDY PARTICIPANT DETAILS

The HMC-1 cell line originated from a patient diagnosed with mast cell leukemia. These cells were extracted from the patient's peripheral blood and successfully cultivated them as continuously dividing clones in laboratory conditions. Additionally, these cells were able to form solid mast cell tumors when introduced into nude mice. DOIs are listed in the key resources table.

The human pancreatic stellate cells (HPSCs) were obtained from a patient undergoing surgery for pancreatic adenocarcinoma. These cells were isolated in primary culture from the surgical sample. To create a stable, long-lasting cell line for research purposes, the isolated PSCs underwent an immortalization process. DOIs are listed in the key resources table.

The co-culture of HMC-1 conditional medium with HPSC was used for tryptase activity assay created in the author's group.[7]

METHOD DETAILS

Computational analysis

Digital consents for the profiling of sequence alignments, structural predictions, gene ontology (GO) terms prediction, enzymes commission (EC) numbers prediction, predicted ligand binding sites and respective ligands, predicted enzyme-substrate pair, and small molecule inhibitors for enzymes were obtained from open access online services.

Sequences associated analyses were performed on web server of Dr. Yang Zhang's research group (https://zhanggroup.org/).[28,29] Multiple sequence alignments were executed on tryptases α, β, δ, γ, and ε utilizing DeepMSA (version 2).[29] Predicted models of tryptases α, β, δ, γ, and ε generated by DMFold deep learning-based approach,[28,29] and the top-scoring 4 to 5 models were then assigned with pLDDT scores, and highest score models were selected to perform subsequent prediction and screening. GO terms, inclusive of molecular function, biological process, and cellular component, were predicted also using the DMFold approach. Each GO term was assigned with a $Cscore^{GO}$, where a higher value indicates a better confidence in predicting the function. Concurrently, Enzymes Commission (EC) numbers, along with $Cscore^{EC}$

and TM-score, were estimated by DMFold approach. Meanwhile, for exploring more, we also predict EC numbers using a refined algorithm in predicting enzyme function developed by Dr. Huimin Zhao, named the CLEAN machine learning model, which is available on the CLEAN platform.[33]

Results obtained by different algorithms provide the possibility to compare EC numbers and their enzyme functions. The enzymes binding sites and their respective small molecule ligands were predicted on the basis of similar protein structure of top-scoring structure models of tryptases α, β, δ, γ, and ε. The high-ranked ligand-binding sites, i.e., high $Cscore^{LB}$, indicate that a more reliable grid could be selected to predict small molecule inhibitors. Enzyme-substrate pairs were predicted through the original Enzyme-Substrate Pair (ESP) model, which developed by Alexander Kroll.[34] Thereafter, small molecule inhibitors for enzymes were screened and analyzed by SiteMap in Schrodinger software (Schrodinger 2018, US),[36,37] a widely recognized platform[47] for the discovery of therapeutic compounds. Upon review, sequences of tryptases α, β, δ, γ, and ε were obtained from the Uniprot database.

Experimental evaluation of tryptase inhibitor efficacy via cell proliferation analysis

Using our previous developed fluorescence-based assay,[5] we assessed the impact of potential tryptase inhibitors on cell division. Human pancreatic stellate cells (HPSCs), authenticated and tested negative for mycoplasma contamination, were first labeled with the intracellular fluorescent tracker CFSE (5 μM) through a 10-min incubation at 37°C. Post-labeling, 25,000 HPSCs were distributed into each well of a 96-well plate. The culture medium was enriched with mast cell-derived conditioned medium and varying concentrations of the candidate compounds identified in Figure S7.

The cells were cultured for 48 h under these conditions. Following this period, HPSCs were collected, washed, and suspended in a solution of phosphate-buffered saline containing 2% fetal bovine serum.

The principle behind this assay is that CFSE fluorescence intensity diminishes with each cell division, as the dye is equally partitioned between daughter cells. We utilized a Beckman Coulter CytoFLEX LX U3-V5-B3-Y5-R3-I2 flow cytometer to measure this fluorescence dilution. The acquired data were subsequently processed using CytExpert software.

To quantify the relative proliferation rates under different experimental conditions, we calculated the median fluorescence intensity (MFI) for each sample. This metric served as a proxy for cell division frequency, allowing us to evaluate the effectiveness of the tested compounds in inhibiting tryptase-mediated cell proliferation.

QUANTIFICATION AND STATISTICAL ANALYSIS

To assess statistical significance between multiple groups, we conducted a one-way analysis of variance (ANOVA), followed by Tukey's post-hoc test for multiple comparisons. Prior to evaluating statistical significance, we performed normality tests and assessed both intra-group and inter-group variations. This ensured that the assumptions underlying our chosen statistical methods were met. We considered results with p-values below 0.05 to be statistically significant. All experiments were independently repeated at least three times to ensure reproducibility, with representative results presented in our findings.